A Novel Finite Element Mesh Truncation Technology Accelerated by Parallel Multilevel Fast Multipole Algorithm and its Applications

Sheng Zuo [1], Yu Zhang [1], Daniel G. Doñoro [1], Xunwang Zhao [1], and Qifeng Liu [2]

[1] Shaanxi Key Laboratory of Large Scale Electromagnetic Computing
Xidian University, Xi'an, Shaanxi 710071, China
yuzhang@mail.xidian.edu.cn

[2] Science and Technology on Electromagnetic Compatibility Laboratory
China Ship Development and Design Center, Wuhan 430064, China

Abstract ─ In order to meet the highly accurate requirements of nowadays scattering and antenna problems, the finite element method requires the use of very accurate mesh truncations techniques able to absorb any outgoing wave completely. In this paper a novel implementation of the finite element mesh truncation technique called Finite Element-Iterative Integral Equation Evaluation (FE-IIEE) is studied. This method can provide a numerical exact radiation boundary condition while the original sparse and banded structure of the finite element method (FEM) matrix is retained. Also, an efficient parallel multilevel fast multipole algorithm (MLFMA) is included to drastically accelerate the time-consuming near field calculation process required by the truncation technique. In order to achieve a high parallel efficiency, both algorithms have been implemented together from scratch, being able to run over several thousands of CPU cores. Through comparisons with commercial software such as HFSS, the accuracy and efficiency of the method are validated showing excellent performance. Finally, a large 100-elements array antenna with more than 24 million unknowns is effectively analyzed using 2560 CPU cores.

Index Terms ─ Finite element method (FEM), integral equation, mesh truncation technique, multilevel fast multipole algorithm (MLFMA).

I. INTRODUCTION

Nowadays, the analysis of large radiation/scattering problems is of crucial interest in military (and civil) nautical and aeronautical industry. The use of higher working frequencies of modern radars makes the analysis, despite the constant enhancements in computer power, a challenge, especially due to the large electrical sizes of the objects.

Among other numerical techniques, the finite element method (FEM) has demonstrated to be a powerful and flexible computational tool for solving large radiation/scattering problems, even when the models present very complex materials [1, 2]. In order to analyze these open region problems, FEM requires the use of mesh truncation techniques that transform the infinite free space into a finite computation domain [3]. It is important to mention that the truncation methodologies have a great impact on the accuracy and efficiency of FEM, especially scattering objects due to their low RCS levels.

In general, the traditional finite element truncation techniques can be roughly divided into two classes: local mesh truncation technologies such as absorbing boundary condition (ABC) [3] and perfectly matched layers (PML) [4] and global mesh truncation technologies such as the finite element - boundary integral (FE-BI) method [5-7]. The formers are easy to implement, but their computational accuracy is unpredictable because of its dependence on many factors such as the distance away from the objects and the shape of truncation boundary. The latter, although can provide exact radiation boundary conditions, presents a partly full system of equations which makes the use of direct solution methods an impossible task forcing us to employ iterative solution strategies (with the consequence convergence issues).

Under this scenario, a mesh truncation algorithm called finite element-iterative integral equation evaluation (FE-IIEE) is studied in this paper [8-12]. This truncation technique provides an exact radiation boundary condition regardless the distance to the sources of the problem while the original sparse and banded structure of the FEM matrix is retained. The convergence of this method is assured by using a convex truncation boundary, moreover, as the distance of truncation boundary away from the objects is larger, faster rates of convergence are obtained [10]. Due to these advantages, it has been extensively hybridized mainly with high frequency methods in the past decades [8-9]. In recent works, authors have used it for the analysis of the unit cell of infinite array antennas as in [12]. However, its effective

Submitted On: June 4, 2019
Accepted On: August 11, 2019

application in complex and electrically large electromagnetic open region problems is still limited due to the extremely large time-consuming task requires during the near field calculation in the truncation process.

In this paper, a massively parallel efficient version of the multilevel fast multipole algorithm (MLFMA) [13] is employed to overcome this limitation, and drastically accelerate the near field calculation. In order to achieve a high parallel efficiency, both techniques have been implemented together from scratch, being able to run over several thousands of CPU cores. Also, complex numerical examples from real practical applications are analyzed to demonstrate the accuracy and efficiency of the proposed method.

The rest of the paper is organized as follows. The theory of FE-IIEE is presented in Section II. Section III describes the implementation of the parallel MLFMA for near field computing acceleration. Section IV contains the numerical results. Finally, our conclusions are gathered in Section V.

II. BASIC THEORY OF FE-IIEE

Let us start considering a typical FE-IIEE setup for a general radiation or scattering problem as illustrated in Fig. 1. The original infinite computational domain is divided into two overlapping domains: the infinite domain (Ω^{EXT}) exterior to the auxiliary boundary S' which generally is the object surface and a FEM domain (Ω^{FEM}) truncated by the surface S. Thus, the mentioned overlapping region is limited by S' and S. The boundary S may be arbitrarily shaped but typically it is selected to be conformal to S'.

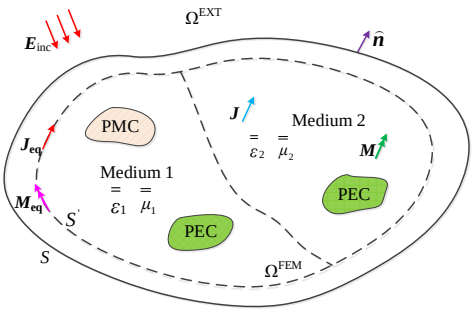

Fig. 1. A typical FE-IIEE method for general radiation or scattering problems.

The distribution of the electric field $\boldsymbol{E}$ in the domain Ω^{FEM} is obtained by solving the following equations:

$$\nabla\times(\bar{\mu}_r^{-1}\cdot\nabla\times\boldsymbol{E})-k_0^2\bar{\varepsilon}_r\cdot\boldsymbol{E}=-\mathrm{j}k_0\eta_0\boldsymbol{J}^{imp} \quad \text{in } \Omega^{FEM}, \tag{1}$$

$$\hat{\boldsymbol{n}}\times\boldsymbol{E}=0 \quad \text{on } \Gamma_{PEC}, \tag{2}$$

$$\hat{\boldsymbol{n}}\times(\bar{\mu}_r^{-1}\cdot\nabla\times\boldsymbol{E})=0 \quad \text{on } \Gamma_{PMC}, \tag{3}$$

$$\hat{\boldsymbol{n}}\times(\bar{\mu}_r^{-1}\cdot\nabla\times\boldsymbol{E})-\mathrm{j}k_0\hat{\boldsymbol{n}}\times(\boldsymbol{E}\times\hat{\boldsymbol{n}})=\boldsymbol{\phi}^{(i)} \quad \text{on } S, \tag{4}$$

where $\bar{\mu}_r$ and $\bar{\varepsilon}_r$ are the relative permeability tensor and relative permittivity tensor of the medium respectively, k_0 represents the wave number in free space, η_0 refers to the free space wave impedance, $\boldsymbol{J}^{imp}$ is an impressed electric current excitation in the FEM domain, j denotes the imaginary unit, and $\hat{\boldsymbol{n}}$ is the external normal unit vector of the corresponding surface. Equations (2), (3), and (4) describe Dirichlet, Neumann and Cauchy boundary conditions, respectively.

The FE-IIEE method starts its execution calculating the electric field $\boldsymbol{E}$ in the Ω^{FEM} domain by solving the system of equations introduced previously. Then, the residual of the Cauchy boundary condition expressed in (4) ($\boldsymbol{\phi}^{(i)}$ term) is updated using the resulted electric field $\boldsymbol{E}$, the equivalent electric current $\boldsymbol{J}_{eq}$ and the equivalent magnetic current $\boldsymbol{M}_{eq}$ on the boundary S'. These currents are used to calculate the electric field $\boldsymbol{E}$ field and its curl over the truncation boundary S. Thus, the residual $\boldsymbol{\phi}^{(i)}$ is updated and a new iteration of the algorithm starts. This process continues until the residual $\boldsymbol{\phi}^{(i)}$ satisfies an end condition (typically an error lower than 1e-5) that implies that the electromagnetic waves reaching the boundary S are completely absorbed.

It is worth mentioning that the initial value of the residual $\boldsymbol{\phi}^{(0)}$ is zero for radiation problems. For scattering problems, the initial value of the residual $\boldsymbol{\phi}^{(0)}$ is the result of evaluating (4) with $\boldsymbol{E}=\boldsymbol{E}^{inc}$ being $\boldsymbol{E}^{inc}$ the incident electric field over the boundary.

The variational formulation of the problem described previously is:

$$\begin{aligned}&\text{Finding } \boldsymbol{E}\in\mathbf{H}(curl;\ \Omega^{FEM})\\&\iiint_\Omega\nabla\times\boldsymbol{v}\cdot(\bar{\mu}_r^{-1}\cdot\nabla\times\boldsymbol{E})dv\\&-k_0^2\iiint_\Omega\boldsymbol{v}\cdot\bar{\varepsilon}_r\cdot\boldsymbol{E}dv+\mathrm{j}k\oiint_{\Gamma_S}(\hat{\boldsymbol{n}}\times\boldsymbol{v})\cdot(\hat{\boldsymbol{n}}\times\boldsymbol{E})ds\\&=\underbrace{-\mathrm{j}k_0\eta_0\iiint_\Omega\boldsymbol{v}\cdot\boldsymbol{J}^{imp}dv-\iint_{\Gamma_P}\boldsymbol{v}\cdot\boldsymbol{\phi}^{P}ds}_{b_I}+\underbrace{(-\oiint_{\Gamma_S}\boldsymbol{v}\cdot\boldsymbol{\phi}^{(i)}ds)}_{b_\phi}\\&\forall\boldsymbol{v}\in\mathbf{H}(curl;\ \Omega^{FEM}),\end{aligned} \tag{5}$$

where $\mathbf{H}(curl;\ \Omega^{FEM})$ is the space of square integrable vector functions with square integrable curl, b_I term corresponds to the internal excitations, and b_ϕ term is related to the residual $\boldsymbol{\phi}^{(i)}$ value of equation (4). The discretization of the above variational formulation is achieved by using second order tetrahedral curl-conforming basis functions that constitute a rigorous implementation of Nédélec first family of finite elements [14, 15].

According to (5), the final FE-IIEE system can be expressed in matrix equation block form as follows,

$$\begin{bmatrix}\boldsymbol{K}_{II} & \boldsymbol{K}_{IS}\\ \boldsymbol{K}_{SI} & \boldsymbol{K}_{SS}\end{bmatrix}\begin{bmatrix}\boldsymbol{g}_I\\ \boldsymbol{g}_S\end{bmatrix}=\begin{bmatrix}\boldsymbol{b}_I\\ \boldsymbol{b}_\phi\end{bmatrix}, \tag{6}$$

where subscripts I and S represent the degree of

freedoms (DOFs) in interior domain and the DOFs on the boundary *S*, respectively. It is important to note that the original sparse and banded structure of the FEM matrix is retained since the integral equation effects (full dense equation blocks) are moved to the right-hand side ($\boldsymbol{b}_{\phi}$ term). In addition, the numerical cost of the second and subsequent iterations is very small since the factorization of the FEM matrix is performed only once at the first iteration (if direct solvers are used).

III. IMPLEMENTATION OF PARALLEL MLFMA FOR NEAR FIELD COMPUTATION

A. Implementation principle of MLFMA accelerated near field calculation

As mentioned in the introduction, the FE-IIEE method still has a limitation due to the extremely large time-consuming task required during the truncation process. FE-IIEE needs to calculate the electric field distribution and its curl over the external boundary *S* using the following integral equations:

$$\boldsymbol{E} = -\mathrm{j}\omega\mu \iint_{S'} \boldsymbol{J}_{\mathrm{eq}} \cdot (\bar{\boldsymbol{I}} + \frac{\nabla\nabla}{k^2}) \cdot G(R) ds' + \iint_{S'} \boldsymbol{M}_{\mathrm{eq}} \times \nabla G(R) ds', \quad (7)$$

$$\nabla \times \boldsymbol{E} = -\mathrm{j}\omega\mu \nabla \times \iint_{S'} G(R) \boldsymbol{J}_{\mathrm{eq}} ds' - \omega^2 \mu\varepsilon \iint_{S'} \boldsymbol{M}_{\mathrm{eq}} \cdot (\bar{\boldsymbol{I}} + \frac{\nabla\nabla}{k^2}) \cdot G(R) ds', \quad (8)$$

where $\bar{\boldsymbol{I}}$ represents the unit dyad, $G(R)$ is the Green's function for the free-space. The computational complexity of the (7) and (8) is O(*MN*) where *M* and *N* are the number of Gaussian sampling points on boundary *S*' and *S* respectively. The numerical cost of this process becomes extremely large when the electrical size of the model increases.

As a fast algorithm, the MLFMA has been widely used in accelerating matrix-vector operations for the method of moment (MoM). Therefore, in order to overcome the current computational bottleneck presented in the FE-IIEE, seems natural to extend the MLFMA and accelerate (7) and (8). Specific details about the MLFMA implementation used in this paper are described next.

Let us consider the two-dimensional problem depicted in Fig. 2. Firstly, the space that contains the field points and the source points is divided into small boxes by levels: the largest box is the level 0 (which surrounds the whole computational domain), then level 0 is divided into smaller boxes obtaining the level 1 and later the level 1 is divided obtaining the level 2. This process continues until the smallest box meets the standard (generally, when the side length is less than 0.5 wavelength).

Accordingly, the smallest boxes at the lowest level (here is level 3), contain three different types of non-empty group: the group with both field and source points, the group only with field points and the group only with source points. In the current implementation in this paper, different groups are marked with different ***Iflag*** values to avoid empty loops and invalid calculations, as displayed in Fig. 2.

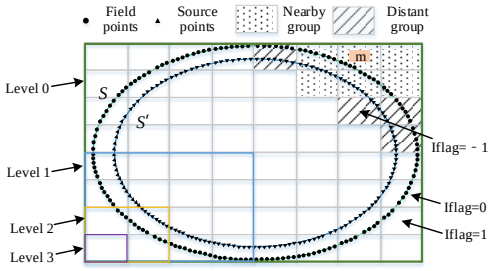

Fig. 2 Configuration for MLFAM based near-field computation.

Through the application of MLFMA, the near field computation in any non-empty groups which contains field points is divided into two categories: the field due to the nearby groups computed using (7) and (8); and, the far-region actions that are calculated through the expansion of the Green's function in (7) and (8) into multipole forms by using the addition theorem and the plane wave expansion theory. After mathematical deduction we obtain that [16],

$$\boldsymbol{E} = -\frac{k^2}{(4\pi)^2}[\eta \iint_{4\pi} \mathrm{e}^{-\mathrm{j}\boldsymbol{k}\cdot(\boldsymbol{r}-\boldsymbol{r}_m)} T_L(kR_{m'm}, \hat{\boldsymbol{k}} \cdot \hat{\boldsymbol{R}}_{m'm})(\bar{\boldsymbol{I}} - \hat{\boldsymbol{k}}\hat{\boldsymbol{k}})\, \boldsymbol{J}_{m'}(\hat{\boldsymbol{k}})\, d^2\hat{\boldsymbol{k}} - \iint_{4\pi} \hat{\boldsymbol{k}} \times \mathrm{e}^{-\mathrm{j}\boldsymbol{k}\cdot(\boldsymbol{r}-\boldsymbol{r}_m)} T_L(kR_{m'm}, \hat{\boldsymbol{k}} \cdot \hat{\boldsymbol{R}}_{m'm}) \boldsymbol{M}_{m'}(\hat{\boldsymbol{k}}) d^2\hat{\boldsymbol{k}}], \quad (9)$$

$$\nabla \times \boldsymbol{E} = \frac{\mathrm{j}k^3}{(4\pi)^2}[\eta \iint_{4\pi} \hat{\boldsymbol{k}} \times \mathrm{e}^{-\mathrm{j}\boldsymbol{k}\cdot(\boldsymbol{r}-\boldsymbol{r}_m)} T_L(kR_{m'm}, \hat{\boldsymbol{k}} \cdot \hat{\boldsymbol{R}}_{m'm})\, \boldsymbol{J}_{m'}(\hat{\boldsymbol{k}})\, d^2\hat{\boldsymbol{k}} + \iint_{4\pi} \mathrm{e}^{-\mathrm{j}\boldsymbol{k}\cdot(\boldsymbol{r}-\boldsymbol{r}_m)} T_L(kR_{m'm}, \hat{\boldsymbol{k}} \cdot \hat{\boldsymbol{R}}_{m'm})(\bar{\boldsymbol{I}} - \hat{\boldsymbol{k}}\hat{\boldsymbol{k}}) \boldsymbol{M}_{m'}(\hat{\boldsymbol{k}}) d^2\hat{\boldsymbol{k}}], \quad (10)$$

where $\hat{\boldsymbol{k}}$ is the unit vector of plane wave expansion direction, $\boldsymbol{r}$ represents the field point coordinates, $\boldsymbol{r}_m$ refers to the center of filed point group, $\boldsymbol{J}_{m'}(\hat{\boldsymbol{k}})$ and $\boldsymbol{M}_{m'}(\hat{\boldsymbol{k}})$ are the radiation pattern of the electric current and magnetic current, respectively, $\boldsymbol{r}'$ is the source point coordinates, $\boldsymbol{r}_{m'}$ denotes the center of source point group, and $T_L(kR_{m'm}, \hat{\boldsymbol{k}} \cdot \hat{\boldsymbol{R}}_{m'm})$ is the translator operator between source point group m' and field point group *m*. By using such a scheme, the computational complexity for updating the residual $\boldsymbol{\phi}^{(i)}$ on the boundary *S* can be reduced from O(*MN*) to $O(\sqrt{MN}\log(MN))$. Figure 3 shows the flowchart of the presented mesh truncation technique where the FE-IIEE and the MLFMA algorithms are working together.

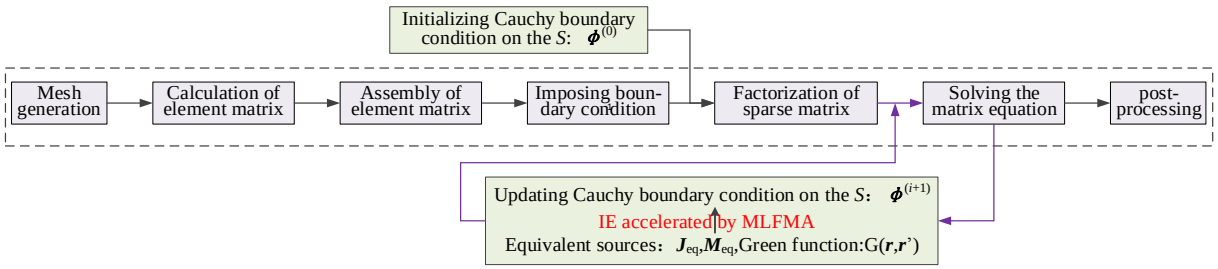

Fig. 3. The program design flow of the FE-IIEE+MLFMA implemented in this paper.

B. Parallel strategy

The parallelization process of MLFMA has two basic partitioning strategies: spatial partitioning and direction partitioning [17]. The former refers to the division of all non-empty groups in each level to each MPI (Message Passing Interface) process, and the latter refers to the distribution of the wave plane directions belonging to each group into the different MPI process. The simple use of one of these strategies usually fails when scaling on a large number of CPU cores. Therefore, in order to improve the scalability of parallel MLFMA, these two parallel partitioning strategies must be combined together.

Considering that the plane wave expansion of the electromagnetic current sources is the most time-consuming process during the nearfield calculation, the non-empty groups in lowest level are firstly divided into N_p portions according to the bisecting source point's rule, where N_p is the number of processes. Each portion is distributed to one MPI process. As an example, Fig. 4 shows the case that the tree nodes from level 2 to level 4 are distributed to 6 processes, where the process indices are denoted by P_0~P_5. It can be seen that the non-empty group (the tree node) at a certain level may be shared by different processes except those at the lowest level. If the non-empty group exists in many processes, its corresponding outgoing and incoming plane wave directions are equally distributed among the related processes. This adaptive partitioning strategy makes our parallel MLFMA to have no special requirements when choosing the number of processes.

On the other hand, it is worth pointing out that during the translation period, if the outgoing plane waves are not in the current process, they need be received from the source group processes where they are located. However, for the near field calculation, we only need to consider the actions from the source points to the field points, in other words, the translation process does not need to be reciprocal. Thus, to avoid invalid communications messages when exchanging outgoing plane waves, a send list and a receive list are established in an earlier stage. The lists include the non-empty group indices, destination and source process indices, and the related outgoing plane wave directions.

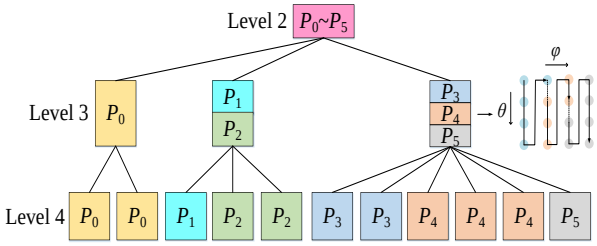

Fig. 4. The parallel strategy of MLFMA for near field computation.

IV. NUMERICAL RESULTS

In this section, the results of different numerical examples are analyzed to demonstrate the performance, versatility and accuracy of the proposed method. Comparisons with well-known commercial software such as ANSYS HFSS [18] and FEKO [19], with in-house codes and with experimental measurements are done to validate its results.

Two different computer platforms are used to complete these simulations: the first one is a Dell T7600 workstation with four 6-core 64-bit E5-2620 0 @2GHz CPUs and 192 GB of RAM; the second one is a Sugon HPC cluster with 548 compute nodes where each node has two 32-core AMD HygonGenuine 2.0 GHz processors (32×512 KB L2 Cache and 64 MB L3 Cache) and 256 GB RAM. The compute nodes are connected with InfiniBand switches to provide the highest communication speeds.

A. Low scattering carrier

The bistatic radar cross-section (RCS) analysis of a metal low scattering carrier object is considered first. Figure 5 shows the low scattering carrier model used in this benchmark.

The model is illuminated by a negative *x*-axis incident *y*-axis polarized uniform plane wave at 3.0 GHz. The overall dimensions of the model are 0.731 m by 0.524 m by 0.077 m corresponding to an electrical size of 7.31 λ by 5.24 λ by 0.77 λ. It is worth noting that due to the low scattering characteristics of the object, certain angles present very low RCS levels which are very difficult to catch numerically. For that reason, authors

consider that this model is a good benchmark to verify the level of accuracy of the proposed truncation technique.

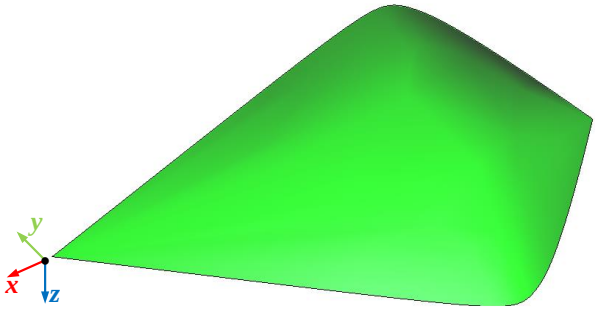

Fig. 5. The metal low scattering carrier model.

The results given by the presented FE-IIEE+MLFMA technique are compared with those given by ANSYS HFSS, FEKO and an in-house higher order method of moments (HOMoM) solver [20]. In order to perform a full comparison with HFSS, all the truncation techniques available in this software, such as ABC, PML and FE-BI, are used in the analysis. The truncation boundary is placed at 0.2 λ from the target in the proposed method. In the case of HFSS, the truncation distance is left to its default option (0.333 λ). The other techniques use method of moments, so no truncation boundary is needed.

Figure 6 shows the comparison between FEKO, the in-house HOMoM code and the proposed FE-IIEE+MLFMA method. An excellent agreement is appreciated even for lowest RCS levels. The results of the pure FE-IIEE method without acceleration are also plotted. In this way, we can see how there are no differences between both versions of the FE-IIEE method indicating that the use of the MLFMA algorithm does not result in any loss of numerical accuracy. However, as it may be seen later, the use of the proposed FE-IIEE+MLFMA technique drastically reduces the total computational time of the analysis.

The comparisons between the results given by HFSS using ABC, PML, and FE-BI as mesh truncation techniques and the proposed method are shown in Fig. 7. In this case, the adaptive convergence accuracy of HFSS was set to 10^{-3}. As aforementioned, the model presents very low RCS values in certain angles that are difficult to catch numerically. In the case of the proposed method, the RCS values for these low level angles present an excellent agreement compared with the levels given by MoM. However, in the case of HFSS, there is a loss of accuracy and cannot match the required RCS levels. It is worth noting that a lower adaptive converge value (lower than 10^{-3}) could mitigate this problem, however the amount of computational resources required to perform the simulation, makes this task almost impossible to conclude.

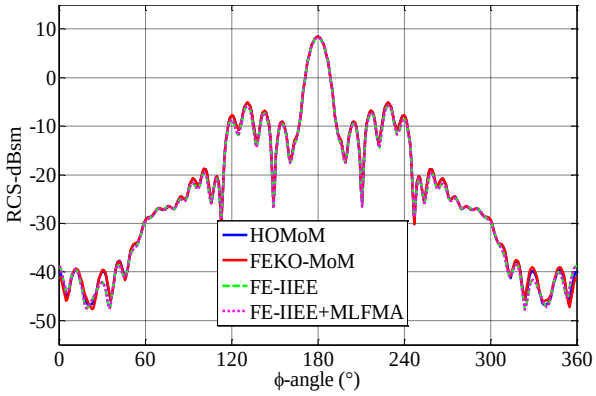

Fig. 6. Bistatic RCS results of the low scattering carrier at 3.0 GHz in the *xoy*-plane calculated by the proposed method and MoM.

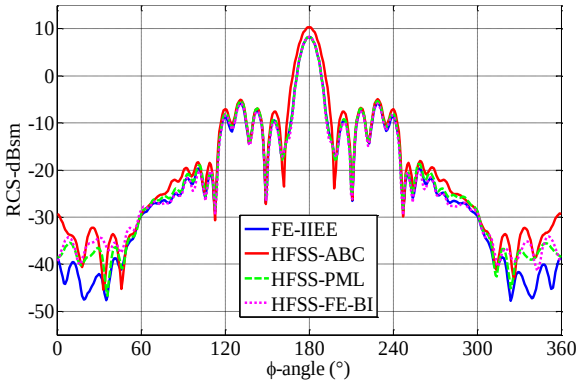

Fig. 7. Bistatic RCS results of the low scattering carrier at 3.0 GHz in the *xoy*-plane calculated by the HFSS and the proposed method.

The computational statistics for these simulations are given in Table 1. All simulations were performed using 12 CPU cores in the Dell T7600 workstation platform described above. It is worth pointing out that the residual value for the proposed method corresponds to the residual of the boundary condition given in (4) meanwhile the residual value for HFSS is its adaptive convergence accuracy. According to this data, we can see how the proposed parallel FE-IIEE+MLFMA technique drastically accelerates the simulation time while the memory level remains unchanged.

Table 1: Computational statistics of the proposed method and HFSS for the low scattering carrier

Methods	Residual	Iteration Count	Number of Tetrahedrons	Unknowns	Memory/ GB	CPU Time/s
FE-IIEE	10^{-4}	8	104,261	710,500	12.57	1639
FE-IIEE+MLFMA	10^{-4}	8	104,261	710,500	12.57	190
HFSS-ABC	10^{-2}	14	208,479	1,236,430	12.28	1100
	10^{-3}	24	2,024,208	12,458,342	154.20	42,406
HFSS-PML	10^{-2}	16	479,470	2,894,550	56.50	9291
	10^{-3}	20	1,429,104	7,069,446	148.30	27,283
HFSS-FE-BI	10^{-2}	12	92,271	586,264/30,078	2.75	924
	10^{-3}	26	1,949,894	13,324,482/290,406	121.70	22,664

B. Waveguide narrow-edge slot antenna

In order to perform a further verification of the computational accuracy and efficiency of the proposed method, the radiation analysis of a waveguide narrow-edge slot antenna is considered next. The model of this antenna is depicted in Fig. 8.

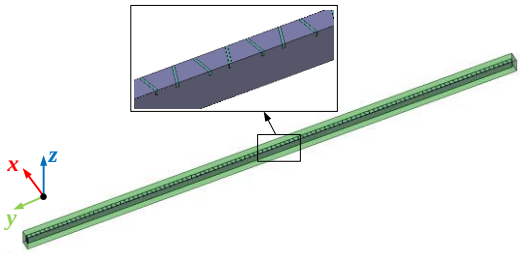

(a)

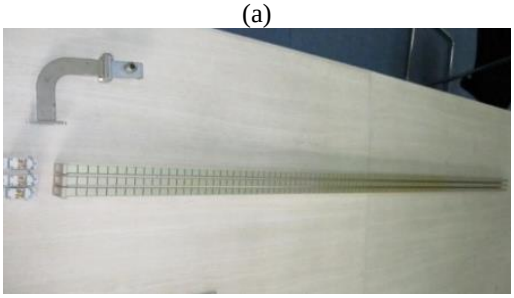

(b)

Fig. 8. The waveguide narrow-edge slot antenna model: (a) the simulation model, and (b) the measurement model.

The waveguide is a WR-90 waveguide (X-band), with dimensions of 22.86 mm by 10.16 mm, and a wall thickness of 1.00 mm. The operation frequency is 9.35 GHz and the rectangular wave ports placed on both ends of the waveguide are used to excite/match the antenna. The total number of tetrahedron used in the discretization of the model is 634,756 and the total number of unknowns is 4,055,352. This simulation is performed using 20 CPU cores in Dell T7600 workstation platform. The residual of the FE-IIEE truncation method is set to 10^{-3}.

In this case, the results are compared with measurement and those given by the in-house HOMoM code. Figure 9 shows the normalized radiation pattern where a very good agreement between the results is appreciated. Table 2 summarizes the computational statistics of this example when using the FE-IIEE and the FE-IIEE+MLFMA method. It is worth noting that, for this moderate electrical size model, the near-field calculation takes more than 97% computation time of FE-IIEE before the MLFMA acceleration is adopted. The use of the proposed hybrid technique drastically reduces the computation time from 5777.6s to 238.4s taking the FE-IIEE capabilities to a higher level.

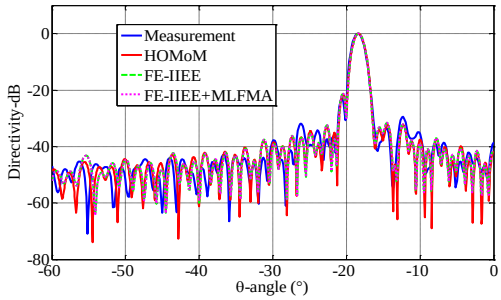

Fig. 9. Normalized radiation pattern of the waveguide narrow-edge slot antenna in the *yoz*-plane.

Table 2: Computational statistics of the FE-IIEE method and FE-IIEE+MLFMA method for the waveguide narrow-edge slot antenna

Methods	Iteration Count	Near Field Calculation Time/s	Total Time/s
FE-IIEE	8	5777.6	5916.2
FE-IIEE+MLFMA	8	238.4	374.1

C. 100-elements array antenna

A very common and typical application of FEM is the analysis of antenna arrays with complex materials and shapes. For this last example, the analysis of a large patch antenna array with 100 elements in a 5 by 20 configuration is considered. Figure 10 shows the unit structure (a) and the whole antenna array (b).

The relative permittivity of the dielectric substrate is 2.65 with a delta tangent of 0.003. Each antenna unit is

fed through two coaxial cables at the bottom in equal amplitude and phase. The operation frequency is 3.2 GHz. The total number of tetrahedron for this antenna is 3,839,140, obtaining a total number of unknowns of 24,530,828. The residual of the FE-IIEE truncation method is set to 10^{-3}. A total of 2560 CPU cores in Sugon HPC cluster were used to perform this simulation which took 3.65 hours and 6.85 TB of memory.

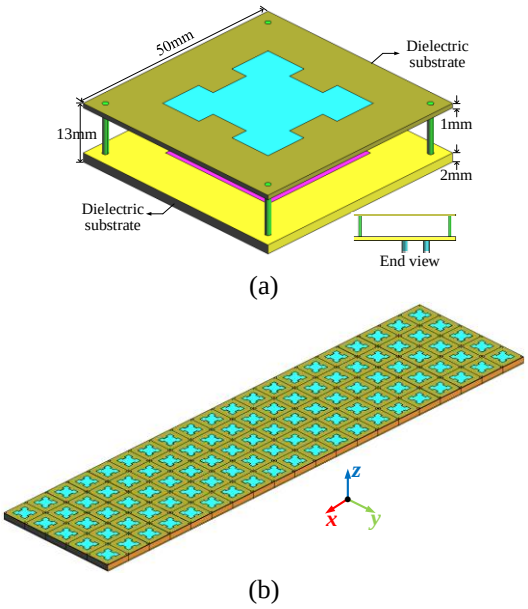

Fig. 10. The array antenna model: (a) the array unit structure, and (b) the array structure.

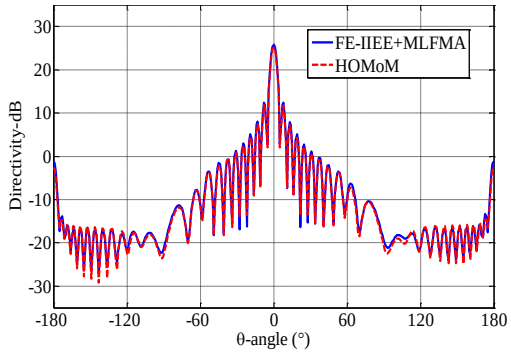

Fig. 11. Radiation pattern of the 100-elements array antenna in the *xoz*-plane.

Figure 11 shows the comparison of the radiation pattern for the elevation cut (*xoz* plane) between FE-IIEE+MLFMA and the in-house higher order method of moments (HOMoM) code. A very good agreement is appreciated confirming that the proposed method can efficiently perform full-wave simulation of challenging electromagnetic problems.

V. CONCLUSION

In this paper, a very efficient parallel FEM mesh truncation technique is presented for the truncation of radiation and scattering problems. This method provides a numerical exact radiation boundary condition while the original sparse and banded structure of the finite element method (FEM) matrix is retained. The accuracy and effectiveness of the proposed technique are demonstrated through the analysis of several practical applications. Specially, the proposed method has shown better accuracy and efficiency than the commercial software HFSS in the analysis of the low scattering objects. As a final conclusion, authors believe that this truncation method is able to meet the highly accurate requirements of nowadays scattering and antenna problems.

ACKNOWLEDGMENT

This work was supported in part by the National Key Research and Development Program of China under Grant 2017YFB0202102, in part by the National Key Research and Development Program of China under Grant 2016YFE0121600, in part by the Fundamental Research Funds for the Central Universities (XJS190210), in part by the Key Research and Development Program of Shandong Province under Grant 2015GGX101028, and in part by the Special Program for Applied Research on Super Computation of the NSFC-Guangdong Joint Fund (the second phase) under Grant No.U1501501.

REFERENCES

[1] J. Jianming, *The Finite Element Method in Electromagnetics*. New Jersey: John Wiley & Sons, 2002.

[2] M. Salazar-Palma, T. K. Sarkar, L. E. Garcia-Castillo, T. Roy, and A. R. Djordjevic, *Iterative and Self-Adaptive Finite-Elements in Electromagnetic Modeling*. Norwood, MA: Artech House Publishers, Inc., 1998.

[3] B. Engquist and A. Majda, "Absorbing boundary conditions for numerical simulation of waves," *Proceedings of the National Academy of Sciences*, vol. 74, no. 5, pp. 1765-1766, 1977.

[4] J. Y. Wu, D. M. Kingsland, J. F. Lee, et al., "A comparison of anisotropic PML to Berenger's PML and its application to the finite-element method for EM scattering," *IEEE Transactions on Antennas and Propagation*, vol. 45, no. 1, pp. 40-50, 1997.

[5] X. Q. Sheng and Z. Peng, "Analysis of scattering by large objects with off-diagonally anisotropic material using finite element-boundary integral-multilevel fast multipole algorithm," *IET Microwaves, Antennas & Propagation*, vol. 4, no. 4, pp. 492-0, 2010.

[6] J. L. Volakis, J. Gong, and A. Alexanian "A finite element boundary integral method for antenna

RCS analysis," *Electromagnetic*, vol. 14, no. 1, pp. 63-85, 1994.

[7] H. Hu, Y. Tan, B. Zhu, and L. Zhou, "A hybrid FE-BI method using in antenna radiation analysis," *2008 8th International Symposium on Antennas*, Propagation and EM Theory, Kunming, pp. 898-901, 2008.

[8] R. Fernandez-Recio, L. E. Garcia-Castillo, I. Gomez-Revuelto, et al. "Fully coupled multi-hybrid FEM-PO/PTD-UTD method for the analysis of radiation problems," *IEEE Transactions on Magnetics*, vol. 43, no. 4, pp. 1341-1344, 2007.

[9] R. Fernandez-Recio, L. E. Garcia-Castillo, I. Gomez-Revuelto, et al., "Fully coupled hybrid FEM-UTD method using NURBS for the analysis of radiation problems," *IEEE Transactions on Antennas and Propagation*, vol. 56, no. 3, pp. 774-783, 2008.

[10] R. Fernandez-Recio, L. E. Garcia-Castillo, I. Gomez-Revuelto, and M. Salazar-Palma, "Convergence study of a non-standard Schwarz domain decomposition method for finite element mesh truncation in electromagnetics," *Progress In Electromagnetics Research (PIER)*, vol. 120, pp. 439-457, 2011.

[11] D. Garcia-Donoro, S. Ting, A. Amor-Martin, et al., "Analysis of planar microwave devices using higher order curl-conforming triangular prismatic finite elements," *Microwave and Optical Technology Letters*, vol. 58, no. 8, pp. 1794-1801, 2016.

[12] D. Garcia-Donoro, L. E. Garcia-Castillo, T. K. Sarkar, et al., "A non-standard Schwarz domain decomposition method for finite element mesh truncation of infinite arrays," *IEEE Transactions on Antennas and Propagation*, vol. 66, no. 11, pp. 6179-6190, 2018.

[13] A. Tzoulis, T. F. Eibert, "Efficient electromagnetic near-field computation by the multilevel fast multipole method employing mixed near-field/far-field translations," *IEEE Antennas & Wireless Propagation Letters*, vol. 4, no. 1, pp. 449-452, 2005.

[14] A. Amor-Martin, D. Garcia-Donoro, L. E. Garcia-Castillo, et al., "A finite element mesh truncation technique for scattering and radiation problems in HPC environments," *Computing & Electromagnetics International Workshop*, IEEE, 2017.

[15] L. E. Garcia-Castillo and M. Salazar-Palma, "Second-order Nédélec tetrahedral element for computational electromagnetics," *International Journal of Numerical Modelling: Electronic Networks*. Devices and Fields (John Wiley & Sons, Inc.), vol. 13, no. 2-3, pp. 261-287, Mar.-June 2000.

[16] C. W. Chew, *Fast and Efficient Algorithms in Computational Electromagnetics*. Artech House, 2001.

[17] X. Zhao, S. W. Ting, and Y. Zhang, "Parallelization of half-space MLFMA using adaptive direction partitioning strategy," *IEEE Antennas and Wireless Propagation Letters*, vol. 13, pp. 1203-1206, 2014.

[18] HFSS. Accessed: 01/06/2019. [Online]. Available: https://www.ansys.com/products/electronics/ansys-hfss, 2019.

[19] FEKO. Accessed: 01/06/2019. [Online]. Available: https://altairhyperworks.com/product/FEKO, 2019.

[20] Y. Zhang, T. K. Sarkar, Y. Zhao, et al., *Higher Order Basis Based Integral Equation Solver (HOBBIES)*. Wiley Press, USA: New Jersey, 2012.

Sheng Zuo was born in 1992 in Hunan, China. He received the B.S. degree of Electronic Information Engineering and the M.S. degree in Electronics and Communications Engineering from Xidian University in 2014 and 2017, respectively. Since September 2017 he is working toward the Ph.D. degree at Xidian University. His research activities and interests are focused in large-scale parallel finite element computation in complex electromagnetic environment, domain decomposition method and fast multipole method.

Yu Zhang received the B.S., M.S., and Ph.D. degrees from Xidian University, Xi'an, China, in 1999, 2002, and 2004, respectively. He joined Xidian University as a Faculty Member in June 2004. He was a Visiting Scholar and Adjunct Professor at Syracuse University from 2006 to 2009. As Principal Investigator, he works on projects including the project of NSFC. He authored four books, namely Parallel Computation in Electromagnetics (Xidian Univ. Press, 2006), Parallel Solution of Integral Equation-based EM Problems in the Frequency Domain (Wiley–IEEE, 2009), Time and Frequency Domain Solutions of EM Problems Using Integral Equations and a Hybrid Methodology (Wiley, 2010), and Higher Order Basis Based Integral Equation Solver (HOBBIES) (Wiley, 2012), as well as more than 100 journal articles and 40 conference papers.